

## Hot-electron dynamics at Cu(100), Cu(110), and Cu(111) surfaces: Comparison of experiment with Fermi-liquid theory

S. Ogawa, H. Nagano, and H. Petek

*Advanced Research Laboratory, Hitachi Ltd., Hatoyama, Saitama 350-03, Japan*

(Received 10 July 1996; revised manuscript received 5 December 1996)

Lifetimes of hot electrons in the 1.3–3.2-eV energy range at low index surfaces of Cu((100),(110),(111)) are measured by two-photon time-resolved photoemission spectroscopy with <10 fs resolution. Energy dependence of the lifetimes deviates from the  $(E - E_F)^{-2}$  functional form predicted by the standard Fermi-liquid theory for free-electron metals, but a qualitative agreement with the theory is obtained by calculating the  $e$ - $e$  scattering times from the band structure of Cu. However, the magnitude of the calculated lifetimes, assuming Thomas-Fermi screening length, is still about six times smaller than the measured. The failure of the free-electron model in predicting the energy dependence and magnitude of the scattering times is attributed in part to  $d$ -band electrons, which have a maximum density at  $-2$  eV and can participate both in scattering and screening of hot electrons. The measured lifetimes also show a modest dependence on the crystal face, which is not reproduced by the band-structure calculations. The origins of this anisotropy may include coherence effects in the excitation, anisotropies in the  $e$ - $e$  scattering cross sections, a contribution from  $e$ - $p$  scattering to the hot-electron decay, or differences in surface electronic structure. [S0163-1829(97)02113-9]

### I. INTRODUCTION

The creation and dissipation of electronic excitation at surfaces is a key to understanding a variety of chemical and physical phenomena at surfaces. Scattering or absorption of energetic particles such as photons, electrons, ions, or molecules at metal surfaces leads to transient nonthermal electron-hole distributions. Hot carriers also can be generated by large electric fields present in semiconductor devices. Relaxation of hot-electron distributions governs the time scales and efficiency of electronically induced surface processes. Thermalization of hot electrons in metals and at metal surfaces occurs on femtosecond time scales due to efficient electron-electron ( $e$ - $e$ ) scattering with the conduction-band electrons. The electron gas equilibrates with the lattice by electron-phonon ( $e$ - $p$ ) scattering on a longer, but still subpicosecond time scale. Highly energetic electrons in metals are of current interest because of their role in surface chemical reactions and hot-electron damage in semiconductor devices.<sup>1,2</sup> The unique properties of hot electrons can be used in a range of applications such as ultrafast electronic and optoelectronic devices,<sup>3</sup> or electronic catalysis.<sup>4,5</sup> Direct measurements of electron-scattering rates as a function of energy and momentum also are valuable for testing the predictions of calculated scattering rates from many-body theories. However, until recently, electronic relaxation in metals could be studied only by indirect means that measure the scattering length scales, rather than time scales, and are limited to a small energy range near the Fermi surface, or to much higher energies above the vacuum level. Although there is a large body of information on  $e$ - $e$  and  $e$ - $p$  scattering from indirect measurements such as heat and electrical transport at low temperatures,<sup>6</sup> or from linewidths in photoemission spectra,<sup>7</sup> such measurements are indirect, and critically depend on the sample purity and surface quality.

Optical excitation and probing of metal surfaces by ul-

trafast laser pulses makes it possible to generate well-defined nonequilibrium hot-electron distributions, and to time-resolve their relaxation.<sup>8,9</sup> With the currently available laser technology, it is possible to follow hot-electron relaxation with <10 fs time resolution.<sup>10</sup> Two-photon time-resolved photoemission (TPTRP) spectroscopy has been developed to study directly the dynamics of optically excited electrons at metal and semiconductor surfaces.<sup>11</sup> This technique has been applied to direct measurement of hot-electron relaxation in noble and transition metals,<sup>10–15</sup> surface state dynamics on clean and adsorbate-covered metal surfaces,<sup>15–17</sup> and much work on charge carrier dynamics in semiconductors.<sup>11</sup>

The starting point for comparison of experimental hot-electron relaxation rates with theory is the standard Fermi-liquid theory for free-electron metals.<sup>18</sup> However, while in some cases the agreement with the Fermi-liquid theory is good, mostly, the theoretical rates are significantly faster than the experimental.<sup>10–15</sup> For copper, the most widely studied metal by TPTRP, there is a large difference between results obtained in several laboratories, and in some cases with the calculated rates from the Fermi-liquid theory.<sup>10,13,15</sup> It is not clear if the variation in the experimental rates merely reflects different interpretations of the data, or whether the experiments are measuring different physical processes. Since copper has a well-known band structure, and is representative of both noble and transition metals, it is important to make critical comparison between experiment and theory.

This paper presents a systematic study of hot-electron decay rates for Cu(100), Cu(110), and Cu(111) surfaces. Section II describes the TPTRP technique and how the  $e$ - $e$  scattering rates are extracted from the measurements. Section III A gives the experimental lifetimes for hot electrons in the 1.3–3.2-eV range. Significantly, different lifetimes are observed for the different crystal orientations, and the lifetimes are not proportional to  $(E - E_F)^2$  as predicted by the standard Fermi-liquid theory for free-electron metals ( $E - E_F$  is hot-electron energy measured relative to the Fermi energy  $E_F$ ).

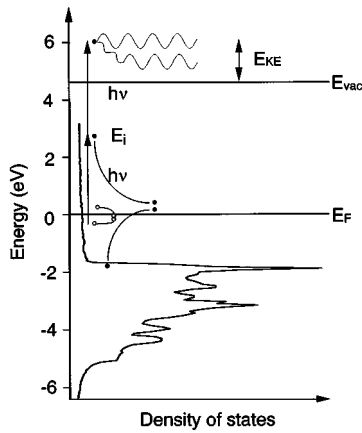


FIG. 1. The principle of two-photon photoemission. One-photon absorption excites electron (●)-hole (○) pairs, with a distribution that is determined by the photon energy, transition moments, and the densities of occupied and unoccupied states (the actual DOS used to model hot-electron lifetimes is shown). Hot-electron dynamics (mainly  $e$ - $e$  scattering) are measured by inducing photoemission of hot electrons with a time-delayed probe pulse. Final-state scattering can interfere with the measurement by changing the  $E_{KE}$  and momentum of a small fraction of the outgoing electrons.

Section III B gives the details of calculations of hot-electron rates from a free-electron model and the band structure of Cu. If the free-electron approximation is assumed, the scattering rates can be calculated from convenient analytic expressions. However, the free-electron model neglects the contributions of  $d$  electrons to scattering and screening. The energy dependence of the rates, but not the magnitude, are brought into much better agreement with the experiment by numerically calculating the rates using the calculated band structure of Cu. Section IV presents a discussion of experimental results on Cu and a comparison with the Fermi-liquid theory. Possible explanations are proposed for why the rates are overestimated by Fermi-liquid theory, and why they may depend on the crystal face.

## II. EXPERIMENT

The process of two-photon time-resolved photoemission by 3.2-eV photons in Cu is schematically shown in Fig. 1. The second harmonic (3.1–3.2 eV) of a homemade Ti:sapphire laser with  $\sim 12$ –18 fs pulsewidth excites electron-hole pairs at the surface within the skin depth of  $\sim 14$  nm. Single-photon absorption generates a hot-electron distribution, which is determined by the photon energy and  $k$ -dependent absorption cross section. Most of the light induces interband transitions from  $d$  bands, starting at  $-2$  eV relative to  $E_F$ , to the  $s,p$  band. However, these hot electrons do not have sufficient energy to be excited above the vacuum level by absorption of another photon, and thus do not contribute to the two-photon photoemission (2PP) signal. Excitation from the occupied  $s,p$  band is not possible by direct interband transitions with 3.2-eV light, but may occur by the phonon or impurity scattering assisted (free-electron) absorption.<sup>19</sup> The hot-electron distribution created by this indirect process is mainly determined by the density of the final states, rather than occurring at specific points in the Brillouin zone (BZ),

as for interband transitions. The absorption cross sections also depend on the incident polarization: 2PP spectra measured with  $p$ -polarized excitation show features due to occupied and unoccupied bands localized at the surface or in the bulk, while with  $s$ -polarization the spectra are mainly due to the bulk. Also, the presence of defects induced by sputtering or oxidation of the surface generally enhances the photoemission yields.<sup>20</sup>

Photoemission of hot electrons with  $\geq 1.3$  eV can be induced by absorption of an additional photon, since the final-state energy is greater than the vacuum level [ $E_{vac}$ : 4.5 eV for Cu(110);<sup>21</sup> 4.6 eV for Cu(100);<sup>22</sup> and 4.9 eV for Cu(111)].<sup>23</sup> Photoelectrons with a specific energy and momentum are detected with a hemispherical energy analyzer. Neglecting any final-state scattering effects, the energy and momentum of the intermediate states  $E_i$  are determined by the photoelectron kinetic energy ( $E_{KE}$ ) and momentum, and the photon energy ( $E_i = E_{KE} + E_{vac} - h\nu$ ). The population dynamics of hot electrons are measured by a two-pulse correlation (TPC) measurement, where a pump pulse creates a hot-electron distribution and an identical time-delayed probe pulse interrogates this distribution by inducing photoemission (see Fig. 2, inset).

The two-photon absorption can be both a coherent or an incoherent process. In the case of coherent two-photon absorption, the TPC time profile will provide information on the polarization dephasing of electron-hole pairs due to both electron and hole scattering. By contrast, in the case of incoherent two-photon absorption, hot electrons do not retain the phase memory of the excitation pulse, and the TPC measures the hot-electron population dynamics within the probed volume. The population decays by the hot-electron scattering with the electrons in the Fermi sea,  $e$ - $p$  scattering, and diffusion into the bulk. A secondary hot-electron population with less than the maximum energy of 3.2 eV is created by a cascade process, whereby a primary hot electron scatters with an electron in the Fermi sea generating two hot electrons with on average  $\frac{1}{2}$  of the total energy of both electrons prior to the collision.<sup>24</sup> Electron-electron scattering will dominate the population dynamics until the electron distribution is thermalized, which typically takes several hundred femtoseconds.<sup>8,9</sup>

The apparatus for TPTRP has been described elsewhere.<sup>10</sup> The second harmonic of the Ti:sapphire laser, which operates at 80 MHz repetition rate and with  $\sim 1$  nJ/pulse energy, is split with a Mach-Zehnder interferometer into an identical pump-probe pulse pair with a variable delay. The two pulses are focused to a spot size of  $\sim 100$   $\mu\text{m}$  on the sample, with a mutual angle of  $< 1^\circ$ . A computer-controlled translation stage translates a retroreflecting mirror pair in one arm of the Mach-Zehnder interferometer in 0.3- $\mu\text{m}$  steps, thereby scanning the pump-probe delay by 2 fs/data point. Repeated scans are averaged for a total integration time of 1–2 s per point. The pulsewidth at the position of the sample can be checked by a noncollinear second-harmonic generation (SHG) autocorrelation (AC) measurement in a  $\beta$ -BaBO<sub>3</sub> crystal mounted on the sample manipulator.  $s$ - or  $p$ -polarized excitation is selected with a zero-order crystalline quartz  $\lambda/2$  waveplate.

Photoemission is measured for clean, single-crystal Cu(100), Cu(110), and Cu(111) surfaces under ultrahigh

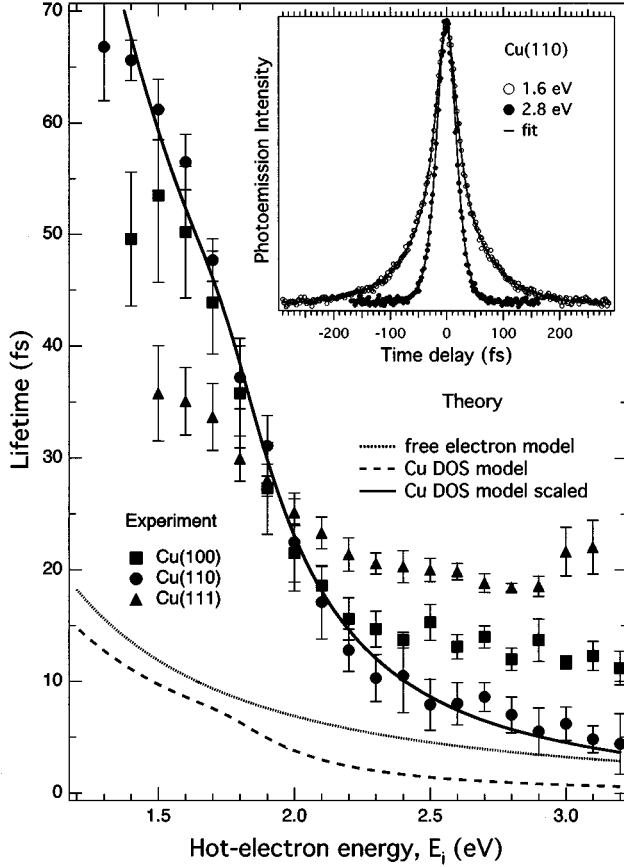


FIG. 2. Experimentally determined hot-electron lifetimes for Cu(100), Cu(110), and Cu(111) surfaces. Calculated lifetimes by Fermi-liquid theory using a free-electron model (dotted line), band-structure model (dashed line), and scaled band-structure model (solid line) are also shown. The inset shows the typical TPC measurements for 1.6- and 2.8 eV hot electrons at the Cu(110) surface. The hot-electron lifetimes are deduced by fitting the data (solid lines) as described in the text.

vacuum conditions with a hemispherical electron energy analyzer. The analyzer is operated with the energy resolution of 100 meV and angular acceptance angle of  $5^\circ$ . The sample orientation is normal to the analyzer and  $30^\circ$  from normal relative to the laser beam. A 2–5-V bias,  $E_{\text{bias}}$  is applied between the sample and analyzer lens to minimize the effects of stray electromagnetic fields. The kinetic energy of the photoelectrons is given by  $E_{\text{KE}} = E_i + h\nu - E_{\text{vac}} + E_{\text{bias}}$ . Although the spectra depend on the  $E_{\text{bias}}$  due to the integration of  $k_{\parallel} \neq 0$  electrons,<sup>20</sup> the TPC scans do not.

### III. RESULTS AND ANALYSIS

#### A. Experimental $e-e$ scattering rates

The inset in Fig. 2 shows typical TPC measurements of hot-electron dynamics at  $E_i$  of 1.6 and 2.8 eV for Cu (110). Near  $\Delta t = 0$ , TPC scans have a fast decay, which is nearly identical at both energies. When the delay is longer than the pulsewidth, there also is a slower decay component (clearly seen for the 1.6-eV electrons), which becomes faster with  $E_i$ . In the analysis of the TPC measurements, the fast and slow components are assigned to coherent and incoherent

two-photon photoemission, which provide the information on the polarization and population decay, respectively.<sup>10</sup> The population decay is attributed to a single  $e-e$  scattering event; however,  $e-p$  scattering, ballistic and diffusive transport out of the volume of observation, and hot-electron cascade also may contribute to the population dynamics. Furthermore, final-state scattering, indicated in Fig. 1, can change the energy and momentum of the outgoing electrons. Thus, the signal is contaminated with a small contribution where  $E_{\text{KE}} < E_i + h\nu - E_{\text{vac}} + E_{\text{bias}}$ . The extent to which these minor processes contribute to the photoemission will be discussed in Sec. IV. The following discussion will focus on the  $e-e$  scattering dynamics.

Because the intensity of the two-photon process is proportional to  $\int |E_{\text{pump}}(t) + E_{\text{probe}}(t - \tau)|^2 dt$ , where  $E(t)$  is the electrical field of the laser, the amplitude of the coherent to incoherent to baseline component in a TPC measurement is 3:2:1, assuming perfect overlap of the pulses and averaging over the optical phase.<sup>10,25</sup> The TPC profiles are modeled by assuming that the optical dephasing is significantly faster than the laser pulse, and therefore the coherent component can be used as a measure of the laser pulse AC. If dephasing were not instantaneous, the coherent component would be broader than the a.c., and it could vary with the hot-electron energy.<sup>26</sup> Where the time scales of the coherent and incoherent components are clearly separated, AC measurement by SHG confirms that the coherent component is equivalent to an *in situ* measurement of the AC.<sup>27</sup> The population decay is extracted by deconvolution of a time-symmetric single exponential decay from the instrument response function given by the AC. Assuming a  $\text{sech}^2$  shape for the excitation pulse gives uniformly the best fit to the TPC measurements at all energies.<sup>10</sup> The lifetimes of hot electrons with 1.3–3.2-eV energy at Cu(100), Cu(110), and Cu(111) surfaces obtained by fitting TPC measurements are plotted in Fig. 2, along with calculated hot-electron lifetimes obtained by three different approaches, which are described in the next section.

#### B. Fermi-liquid theory calculation of $e-e$ scattering rates

The standard theory of  $e-e$  scattering is based on Landau's theory of Fermi liquids. The  $e-e$  scattering rates are calculated from the Fermi-liquid theory by assuming both the free-electron and the actual calculated band structure of Cu. Hot-electron decay is modeled as a scattering process of the electron in the initial state  $\mathbf{k}_1$  with an electron in the Fermi sea,  $\mathbf{k}_2$ , to produce two hot electrons in states  $\mathbf{k}'_1$  and  $\mathbf{k}'_2$ , which conserve energy and momentum. The probability of  $e-e$  scattering has the form<sup>28</sup>

$$P_{\mathbf{k}_1 \mathbf{k}_2}^{\mathbf{k}'_1 \mathbf{k}'_2} = \frac{2\pi}{\hbar} |M_{12}^{1'2'}|^2 \Phi(\varepsilon_1 \varepsilon_2 \varepsilon'_1 \varepsilon'_2) \rho(\varepsilon_1 \varepsilon_2 \varepsilon'_1 \varepsilon'_2), \quad (1)$$

where  $M_{12}^{1'2'}$  is the  $e-e$  scattering matrix element and  $\varepsilon_i$  are the energies of corresponding electron states.  $\Phi$  is the occupation factor, which is equal to 1 when  $\mathbf{k}_1$  and  $\mathbf{k}_2$  are occupied and  $\mathbf{k}'_1$  and  $\mathbf{k}'_2$  are unoccupied, and otherwise zero as required by the Pauli principle.  $\rho$  is the density of states (DOS) that conserves energy. The interaction between the electrons at position  $\mathbf{r}_1$  and  $\mathbf{r}_2$  in the Fermi liquid can be

described by the screened Coulomb potential given in the Fourier series representation by

$$H = \frac{e^2}{\varepsilon_0 \Omega} \sum_{\mathbf{k}} \frac{\exp[i\mathbf{k}(\mathbf{r}_1 - \mathbf{r}_2)]}{\mathbf{k}^2 + q_s^2}, \quad (2)$$

where  $q_s^{-1}$  is the screening length,  $\Omega$  is the volume of the crystal, and  $\varepsilon_0$  is the dielectric constant of vacuum.  $M_{12}^{1'2'}$  is evaluated by the Born approximation<sup>28,29</sup>

$$M_{12}^{1'2'} = \int \psi_{\mathbf{k}_1 \mathbf{r}_1}^* \psi_{\mathbf{k}_2 \mathbf{r}_2}^* H \psi_{\mathbf{k}'_1 \mathbf{r}_1} \psi_{\mathbf{k}'_2 \mathbf{r}_2} d\mathbf{r}_1 d\mathbf{r}_2 \\ = \begin{cases} \frac{e^2}{\varepsilon_0 \Omega} \frac{1}{|\mathbf{k}'_1 - \mathbf{k}_1|^2 + q_s^2} & (\text{for } \mathbf{k}_1 + \mathbf{k}_2 = \mathbf{k}'_1 + \mathbf{k}'_2) \\ 0 & (\text{for } \mathbf{k}_1 + \mathbf{k}_2 \neq \mathbf{k}'_1 + \mathbf{k}'_2), \end{cases} \quad (3)$$

using plane waves for wave functions,  $\psi_{\mathbf{k}, r_i} = (1/\sqrt{\Omega}) \exp(i\mathbf{k}, r_i)$ . The scattering rate of the hot electron in the state  $\mathbf{k}_1$  is given by the sum of probabilities  $P_{\mathbf{k}_1 \mathbf{k}_2}^{\mathbf{k}'_1 \mathbf{k}'_2}$  over all possible states  $\mathbf{k}_2$ ,  $\mathbf{k}'_1$ , and  $\mathbf{k}'_2$ :

$$\tau_{e-e}^{-1}(\mathbf{k}_1) = \sum_{\mathbf{k}_2 \mathbf{k}'_1 \mathbf{k}'_2} P_{\mathbf{k}_1 \mathbf{k}_2}^{\mathbf{k}'_1 \mathbf{k}'_2} \\ = 2 \frac{2\pi}{\hbar} \left( \frac{e^2}{\varepsilon_0 \Omega} \right)^2 \sum_{\mathbf{k}_2 \mathbf{k}'_1 \mathbf{k}'_2} \frac{1}{(|\mathbf{k}'_1 - \mathbf{k}_1|^2 + q_s^2)^2} \\ \times \Phi(\varepsilon_1 \varepsilon_2 \varepsilon'_1 \varepsilon'_2) \rho(\varepsilon_1 \varepsilon_2 \varepsilon'_1 \varepsilon'_2). \quad (4)$$

The multiplicative factor of 2 in Eq. (4) arises from the assumption that the scattering rates between electrons with parallel and antiparallel spins are the same. According to the standard procedure, summation over  $\mathbf{k}_2$ ,  $\mathbf{k}'_1$ , and  $\mathbf{k}'_2$  in Eq. (4) is replaced by the integration over the energy ( $d\varepsilon$ ) and the angular part of Fermi surface ( $dS$ ) with the substitution

$$d\mathbf{k} = \frac{d\varepsilon dS}{\partial\varepsilon/\partial k} = \frac{d\varepsilon dS}{\hbar v(\mathbf{k})}. \quad (5)$$

With the assumption that the scattering process occurs in the vicinity of spherical Fermi surface ( $|\mathbf{k}_1| = |\mathbf{k}_2| = |\mathbf{k}'_1| = |\mathbf{k}'_2| = k_F$ ;  $k_F$  is the Fermi momentum), and by replacing  $\partial\varepsilon/\partial k = \hbar v(k)$  with a constant  $[\hbar v(k_F)]$ , Eq. (4) leads to the result at  $T=0$ :<sup>29</sup>

$$\tau_{e-e}^{-1} = \frac{e^4 k_F^2}{16\pi^3 \hbar^4 \varepsilon_0^2 v^3 q_s^3} \left[ \frac{2k_F q_s}{4k_F^2 + q_s^2} + \arctan\left(\frac{2k_F}{q_s}\right) \right] (E - E_F)^2 \\ = \frac{\pi\sqrt{3}}{64} \omega_p \left[ \frac{2k_F q_s}{4k_F^2 + q_s^2} + \arctan\left(\frac{2k_F}{q_s}\right) \right] \left( \frac{E - E_F}{E_F} \right)^2, \quad (6)$$

where  $\omega_p$  is the plasmon frequency. Equation (6) gives comparable  $e-e$  scattering rates to expressions of Pines and Nozières:<sup>30</sup>

$$\tau_{e-e}^{-1} = \frac{\pi^2 \sqrt{3}}{128} \omega_p \left( \frac{E - E_F}{E_F} \right)^2; \quad (7)$$

and Quinn:<sup>18</sup>

$$\tau_{e-e}^{-1} = 2E_f(k) \\ \approx 2 \frac{e^2}{2a_0} \frac{\pi^{1/2}}{32(\alpha r_s)^{3/2}} \left[ \frac{(\alpha r_s / \pi)^{1/2}}{1 + (\alpha r_s / \pi)} \right. \\ \left. + \arctan\left(\frac{\pi}{\alpha r_s}\right)^{1/2} \right] \left( \frac{E - E_F}{E_F} \right)^2 \frac{k_F}{k} \\ = \frac{\pi\sqrt{3}}{64} \omega_p \left[ \frac{2k_F q_s}{4k_F^2 + q_s^2} + \arctan\left(\frac{2k_F}{q_s}\right) \right] \left( \frac{E - E_F}{E_F} \right)^2 \frac{k_F}{k}, \quad (8)$$

where  $E_f(k)$  is the imaginary part of self energy of quasiparticles with momentum  $k$ ,  $\alpha = (4/9\pi)^{1/3}$ ,  $a_0$  is a Bohr radius, and  $r_s$  is the density parameter. The free-electron approach outlined above may be appropriate for thermally excited electrons near the Fermi surface. However, for hot electrons with  $>2$ -eV energy, Cu 3d electrons, which have the maximum density of states at  $\sim 2$  eV below  $E_F$ , will make the dominant contribution to the scattering rate. To include the effect of  $d$  bands on the scattering rate, Eq. (4) must be solved numerically by calculating the phase space for the scattering process from the actual band structure of Cu, as described next.

The band structure ( $\mathbf{k}, E$ ) of Cu is calculated by an augmented plane wave (APW) method with a Gunnarsson-Lundqvist-type local-density approximation.<sup>31</sup>  $\Gamma(0,0,0) - X(2\pi/a, 0, 0)$  direction ( $a$  is the lattice constant) is divided into eight segments: thus  $16 \times 16 \times 16/2 = 2048$  points are calculated in the first Brillouin zone. In this model, the crystal volume ( $\Omega$ ) corresponds to  $2048a^3/4 = 2.42 \times 10^{-26}$  (m<sup>3</sup>). The scattering matrix element  $M_{12}^{1'2'}$  is calculated by assuming the screening length  $q_{\text{TF}}^{-1}$  from the Thomas-Fermi model:<sup>29</sup>

$$q_{\text{TF}}^{-1} = \left( \frac{e^2}{\varepsilon_0} D(E_F) \right)^{-1/2}, \quad (9)$$

where  $D(E_F)$  is the DOS at the Fermi level.  $D(E_F) = 0.11$  from the free-electron model and 0.15 (states eV<sup>-1</sup> spin<sup>-1</sup> atom<sup>-1</sup>) from the band-structure calculation give  $q_{\text{TF}}^{-1} = 0.55$  and 0.47 Å, respectively.

Since Cu(111) and Cu(100) have band gaps for  $k_{\parallel} = 0$  between  $-0.85$ – $4.1$  eV and  $1.8$ – $7.9$  eV,<sup>32,33</sup> respectively, the intermediate state cannot be associated with a specific bulk band, and therefore the proper choice of momentum  $\mathbf{k}_1$  for the scattering rate calculation is ambiguous. The  $k_{\parallel} = 0$  photoemission may be attributed to either damped band-gap intermediate states or to the final-state scattering from the  $k_{\parallel} \neq 0$  direction.<sup>10</sup> The scattering rate calculation is performed based on two different assumptions for  $\mathbf{k}_1$ . First, the hot-electron momentum  $\mathbf{k}_1$  is assumed to be equal to that of the initial state [ $\Gamma$ -X ( $\Delta_1$ ) band for Cu(100),  $\Gamma$ -K ( $\Sigma_1$ ) for Cu(110), and  $\Gamma$ -L ( $\Lambda_1$ ) for Cu(111)], because the momentum of the photon (3.2 eV) is  $\sim 0.1\%$  of that of the electron, and  $k_{\parallel} = 0$  momentum component is conserved in the photoemission process. Second,  $\mathbf{k}_1$  is assumed to be equal to that of unoccupied  $s$ - $p$  bands ( $\Gamma$ -K,  $\Gamma$ -W, and  $\Gamma$ -U), and the electron scatters into the  $k_{\parallel} = 0$  direction after absorbing the sec-

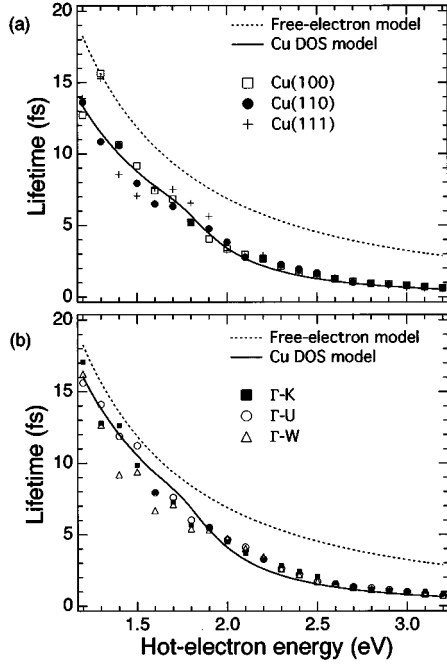


FIG. 3. (a) Calculated lifetimes for the three crystal faces of Cu using the calculated band structure, a screening length of  $q^{-1}=0.465 \text{ \AA}$ , and assuming the hot-electron momentum  $\mathbf{k}_1$  is the same as the initial-state momentum. Dashed line shows lifetimes based on free-electron model with  $q^{-1}=0.55 \text{ \AA}$ . Solid line is a fitted function using the calculated DOS of Cu  $D(\varepsilon)$  (see text). (b) Calculated lifetimes based on the same model as in (a), but assuming the momentum  $\mathbf{k}_1$  of the unoccupied  $s$ - $p$  bands ( $\Gamma$ -K,  $\Gamma$ -W, and  $\Gamma$ -U).

ond photon. To calculate  $e$ - $e$  scattering rates according to Eq. (4),  $\mathbf{k}_2$ ,  $\mathbf{k}'_1$ , and  $\mathbf{k}'_2$  are scanned in the BZ to identify states that satisfy the energy and momentum conservation. Because the  $k$  space is divided into discrete elements, energy and momentum conservation requirements are relaxed from  $\Delta\varepsilon=0$  and  $\Delta k=0$  to  $\Delta\varepsilon \leq 0.2 \text{ eV}$  and  $\Delta k \leq \pi/8a$ .

The two different choices of intermediate state momenta give different calculated lifetimes for each of the crystal faces in Figs. 3(a) and 3(b). Figure 3 also shows a comparison of the calculated lifetimes from the band structure and free-electron models [Eq. (8)], using the parameters of  $r_s=2.67$  and  $E_F=7.0 \text{ eV}$ .<sup>34</sup> The solid line is a function proportional to

$$\int D(\varepsilon_2)D(\varepsilon'_1)D(\varepsilon_1+\varepsilon_2-\varepsilon'_1)d\varepsilon_2d\varepsilon'_1 \\ \propto \sum_{\varepsilon_2\varepsilon'_1\varepsilon'_2} \Phi(\varepsilon_1\varepsilon_2\varepsilon'_1\varepsilon'_2)\rho(\varepsilon_1\varepsilon_2\varepsilon'_1\varepsilon'_2),$$

which represents the phase space for the scattering processes calculated from the DOS of Cu  $[D(\varepsilon)]$ . This function is scaled to give an average of calculated lifetimes for the three faces. The lifetimes in the band-structure model are not very sensitive to  $\mathbf{k}_1$ : the choice of the unoccupied  $s$ - $p$  band momentum [Fig. 3(b)] gives  $\sim 20\%$  longer lifetimes as compared with the initial-state momentum [Fig. 3(a)]. Hot electrons with  $< 2$ -eV energy can scatter only with free-electron-

like  $s$ - $p$  bands. Thus, below 2 eV, the band-structure and free-electron calculations give similar lifetimes, except for a small difference in magnitude (20–25 %). This is due to different calculated values of  $D(E_F)$  and the hot-electron momenta used in the two models. The difference between the free-electron and band-structure calculations is more significant above 2 eV, where 60–70 % of hot electrons decay by scattering with the  $d$ -band electrons. Although the  $d$  bands are more localized, they dominate the DOS below  $-2 \text{ eV}$ . This decay channel, by definition, is not included in the free-electron model.

The experimental and calculated lifetimes are compared in Fig. 2. Both the band-structure and free-electron models have significantly shorter lifetimes than those observed. The magnitude of calculated rates can be brought into better agreement with the experiment by changing the screening length so as to reproduce the data. The solid line in Fig. 2 gives the calculated lifetimes from the band-structure model, assuming the initial-state momentum for  $\mathbf{k}_1$  and a screening length of  $0.27 \text{ \AA}$ . This leads to an excellent agreement between the calculated lifetimes and those for Cu(110), while those for Cu(111) and Cu(100) cannot be reproduced over the whole energy range in this manner. Since the scattering cross section is proportional to  $q^{-2}$ , using the screening length as a variable parameter is a convenient way for changing  $M_{12}^{1/2'}$ . However, the agreement with the data should not be interpreted as an experimental determination of the screening length. Some reasons why the present calculation underestimates the lifetimes will be presented in the next section.

## IV. DISCUSSION

### A. Hot-electron dynamics

In Sec. III, the experimental data are analyzed under the assumption that the TPC measures  $e$ - $e$  scattering dynamics under single-scattering event conditions. Since other factors can contribute to the dynamics, this assumption requires further discussion. Electron-phonon scattering is expected to be much less efficient in hot-electron relaxation because the energy lost per collision is considerably smaller than the energy resolution of the experiment, and more than an order of magnitude smaller than for an  $e$ - $e$  scattering. Experiments on gold films show that the  $e$ - $p$  scattering becomes the dominant electron energy decay process only after several hundred femtoseconds.<sup>12,35</sup> However,  $e$ - $p$  scattering is very anisotropic<sup>36</sup> so there may be regions of the Fermi surface, such as the  $\langle 111 \rangle$  neck, where  $e$ - $p$  scattering may contribute more significantly than in other regions. Temperature dependence studies will be necessary to assess the contribution of  $e$ - $p$  scattering to hot-electron decay rates.

Hot-electron transport out of the skin region into the bulk also will appear as population decay in the probed volume. Comparison of hot-electron decay rates measured by TPTPR for gold films of varying thickness, shows that transport contributes 10–20 % of overall decay at 1.5 eV.<sup>14</sup> Thus, when the scattering length is longer than the skin depth, there will be an increasing contribution from transport to the hot-electron dynamics. Transport may be responsible for the apparent saturation of lifetimes at low energies seen in Fig. 2.

Both  $e$ - $p$  scattering and transport are expected to make an increasingly larger contribution to the loss of hot-electron population with decreasing hot-electron energies. However, population of low-energy hot-electron states by cascade from higher energies is expected to have the opposite effect. The extent of this contribution can be estimated from the scattering calculation performed here. Scattering of a 3.2-eV hot electron with  $d$  bands at  $-2$  eV can generate secondary electrons with a maximum of 1.2 eV, which is below the range of energies investigated here. Only 30–40 % of the hot electrons above 2 eV that scatter with electrons in the  $s,p$  band can generate secondary electrons above 1.3 eV. The scattering calculation shows that the probability of creation of hot-electron population above 1.5 eV by scattering of 3-eV electrons from  $s$ - $p$  and  $d$  bands is  $<7\%$ . Thus, a hot-electron cascade will make a small contribution to the dynamics of the lowest-energy hot electrons, which will compensate, in part, for the loss of population due to the  $e$ - $p$  scattering and transport.

The final-state scattering process also makes a contribution to the TPC measurements, which increase with the decreasing energy of the photoelectrons.<sup>37</sup> The  $E_i$  of the outgoing electrons that lose a substantial amount of energy before escaping into the vacuum cannot be determined from  $E_{KE}$  and  $h\nu$ . Since the signal that is attributed to a specific  $E_i$  will have a contribution from higher-energy hot electrons, the observed lifetimes will be shorter than if the final-state scattering did not occur. The contribution of final-state scattering to the photoemission signal has been determined quantitatively for noble metals under similar conditions.<sup>37</sup> These measurements show that the final-state scattering contribution to the photoemission signals at lowest energies is  $<10\%$ .

From the above discussion it is concluded that the dominant process for hot-electron decay is  $e$ - $e$  scattering. The contributions of  $e$ - $p$  scattering, diffusion, hot-electron cascade, and final-state scattering have the largest contributions to the signal at low photoemission energies. These processes contribute  $\leq 30\%$  to the decay rates of electrons at 1.5 eV. Thus, the present measurements give an upper limit to the  $e$ - $e$  scattering rates. The accuracy of the data at high energies is mostly limited by the accuracy of measuring the instrument response function, and the assumption the optical dephasing is instantaneous. Experiments aimed at establishing the upper limit for the optical dephasing at Cu surfaces are presently under way.<sup>27</sup>

### B. Comparison of experimental results

The results presented in Sec. III are as follows: (i) the  $e$ - $e$  scattering rates are measured at the three low index faces of Cu in the same experiment; and (ii) the rates are calculated from the band structure of Cu, rather than the free-electron model. Therefore it is worthwhile to compare and contrast the present results with the previous measurements on Cu, and to evaluate the predictive power of the Fermi-liquid theory.

Comparison of previous TPTRP measurements on Cu suggests that either there is a substantial dependence of the rates on the crystal face, or there are discrepancies among results obtained in different laboratories. Hot-electron lifetimes were first reported in Ref. 13 for Cu(100), using a similar experimental approach to the present work, but with

lower ( $\sim 50$  fs) time resolution. The TPC measurements had only 2:1 intensity ratio, possibly due to longer pulse widths and incomplete overlap of the pump and probe pulses. As a result, the data were fit without including the coherent component in the TPC analysis. Probably, this is responsible for  $\sim 2$  times shorter lifetimes reported in Ref. 13 as compared with the present work.<sup>10</sup> Otherwise, similar experimental approaches seem to give consistent results.<sup>38</sup>

Hot-electron lifetimes at the Cu(111) surface also have been measured by two-color two-photon time-resolved photoemission spectroscopy in the 0.3–2.2-eV range, by a cross-correlation measurement with 2.23- and 4.45-eV pulses of 65 fs duration.<sup>15</sup> The reported lifetimes are essentially identical to the predictions of the Fermi-liquid theory for a free-electron gas [Eq. (7)]; however, in the energy range where there is an overlap, the lifetimes of Ref. 15 are 3–4 times shorter than the present results. Such short lifetimes also contradict a large body of literature on  $e$ - $e$  scattering from low-temperature transport measurements in Cu, which show that the Fermi-liquid theory for a free-electron gas overestimates the rates by a factor of 3–4 due to  $d$ -band screening and other effects (see below).<sup>39</sup> The surprisingly short lifetimes possibly result from assumptions that were made in the model for analyzing the data: the lifetimes were deduced by modeling the pump-probe measurements with optical Bloch equations for a two-level system, under the assumption that the 2.23- and 4.45-eV light pulses act as the pump and the probe, respectively.<sup>15</sup> Since the pulsewidths were as much as ten times longer than the extracted lifetimes, and the signals contain significant contributions from the hot-electron cascade, the lifetimes were deduced by fitting only the signal rise and delay from an independently determined zero delay time of the pump-probe pulse pair. The lifetimes could be underestimated for the following reasons. (i) A two-color experiment probes the dynamics of two populations separated in energy corresponding to the difference of the two photon energies. However, the analysis in Ref. 15 neglects the process where a 4.45-eV light acts as the pump and a 2.23-eV light is the probe. Since the two pulses were of comparable energy, and the absorption cross section at 4.45 eV is a factor of 2 larger than at 2.23 eV, this excitation pathway should make a considerable contribution to the photoemission signal at short delays. (ii) It is well known that optical Bloch equations are inappropriate for semiconductors due to strong Coulomb interaction in the electron-hole plasma.<sup>40</sup> Many-body effects related to interacting electrons and holes under optical irradiation can be treated by semiconductor Bloch equations.<sup>41</sup> However, the validity of the application of optical Bloch equations to the optical excitation of metals is not established. In particular, treating optical coupling between two continua as a two-level system may not be justified, and to properly describe a two-photon process, a three-level model is required. (iii) A fraction of the signal, particularly at long delays, is attributed to the population of the observed states by the hot-electron cascade. The data were fit only in the rise time to avoid complications due to secondary scattering events. The fits for low-energy electrons suggest that the hot-electron cascade contributes to the signal only after a delay of  $\sim 100$  fs, when most of the hot electrons with  $>1$ -eV energy have already decayed. However, Boltzmann-equation studies of the evolution of hot-

electron distributions in metals show that the rate of filling of low-energy states by hot-electron cascade is fastest at the shortest delay times.<sup>42</sup> Thus it is not possible to separate the time scales of the population of low-energy states by optical excitation and hot-electron cascade when the excitation pulse duration is significantly longer than the hot-electron lifetimes. Yet even though some of these assumptions may lead to an overestimation of the scattering rates, it is not clear whether they can explain such a large difference between the results in Ref. 15 and the present work. One- and two-color experiments may yield different results due to differences in the penetration lengths, hole energies, coherence effects in the excitation process, or other effects. Since time-resolved photoemission is not yet a mature technique, further refinement in experimental procedures and theoretical analysis still is necessary to extract the essential physics from the experiment.

### C. Theoretical analysis

The comparison of experimental and calculated hot-electron lifetimes in Figs. 2 and 3 show that the Fermi-liquid theory (i) qualitatively explains the energy dependence of the lifetimes; (ii) predicts  $\sim 6$  times shorter lifetimes at a given energy; and (iii) does not reproduce the anisotropy in lifetimes. Possible reasons for the discrepancies between experiment and theory are discussed in this section.

The magnitude of experimental and theoretical hot-electron lifetimes can be brought into agreement by assuming a smaller screening length of  $q^{-1}=0.27 \text{ \AA}$ , which implies a smaller scattering matrix element, since according to Eq. (3),  $M_{12}^{1'2'} \sim q^{-2}$ . The overestimation of the rates by the Fermi-liquid theory can be attributed to several approximations. (i) The use of Born approximation gives only the first-order estimate of the scattering matrix element. By the phase-shift method it was shown that the Born approximation overestimates  $M_{12}^{1'2'}$  by  $\sim 2$  in Cu.<sup>43</sup> (ii) Though the  $e-e$  scattering rate is assumed to be independent of the electron spin [Eq. (4)], it may be different for the parallel and antiparallel spins due to the exchange interaction. Scattering rates between antiparallel-spin electrons have been calculated to be about 4–10 times larger than between parallel-spin electrons for a metal such as Cu.<sup>44</sup> This is consistent with the electron-spin relaxation measurements in Ni.<sup>45</sup> (iii) The contribution of the  $3d$  bands to the screening is not included in the free-electron model. To estimate the  $d$ -band screening,  $\epsilon_0$  in Eq. (9) should be replaced with the actual dielectric constant of Cu at zero frequency  $\epsilon=5.6\epsilon_0$ .<sup>46</sup> Since the lifetimes have a  $\sim \sqrt{\epsilon}$  dependence on the dielectric constant, which is used to calculate both the screening length and scattering cross section [Eqs. (3), (5), and (9)], this will increase the lifetimes by 2.4.<sup>47</sup> (iv) Umklapp processes, which are not considered in the present calculation, have been shown to decrease  $e-e$  scattering rates by 16–30 % in Al.<sup>48</sup> Thus, the difference between the calculated and experimental hot-electron lifetimes can be expected from the approximations used in calculating the scattering matrix elements.

The present calculation shows that the dependence of the scattering rate on the initial or intermediate state  $\mathbf{k}$  is smaller than the observed anisotropy in the rates. The face-dependent

lifetimes may be due to the anisotropies in  $e-e$  and  $e-p$  scattering cross sections. Anisotropic scattering cross section can be obtained by evaluation of Eq. (3) with realistic (anisotropic) wave functions rather than plane waves.<sup>29</sup> Radio-frequency size effect measurements on Cu show that the  $e-e$  scattering rates are  $\sim 20\%$  larger for orbits about the  $\langle 111 \rangle$  direction as compared to the  $\langle 100 \rangle$  direction supporting the existence of anisotropy in  $e-e$  scattering rates.<sup>49</sup> Since  $e-p$  inelastic collisions are dominated by small-angle scattering, the rates show much larger anisotropy than for  $e-e$  collisions. The  $e-p$  scattering rates differ by more than a factor of 30, being slowest for the electron orbits in the plane perpendicular to the  $\langle 110 \rangle$  orientation, intermediate for belly orbits about  $\langle 100 \rangle$ , and fastest for orbits on the neck about  $\langle 111 \rangle$ .<sup>29,50</sup> Thus, an anisotropy in the  $e-e$  scattering rates and a significant contribution from the anisotropic  $e-p$  scattering could explain the trends for low hot-electron energies ( $< 2.0$  eV), where the decays are fastest for Cu(111) and slowest for Cu(110).

Since lifetimes are determined by the interaction between the intermediate states and their immediate electronic environment, another factor that may contribute to the anisotropy is the presence of a surface. The photoemission signal is not resonant with the bulk bands. The dependence of the photoemission yields on the polarization and surface conditions suggests a strong contribution from the surface. Surface effects can result in crystal face dependence through differences in the surface electronic structure or on account of band gaps at  $k_{\parallel}=0$  for Cu(100) and Cu(111). The positions of the  $d$  bands at the surface increase in energy and their widths decrease in comparison with the bulk. This trend is least for the close-packed Cu(111) and largest for the most open-packed Cu(110).<sup>51</sup> When the  $d$ -band energy and density increase, more  $d$ -band electrons can contribute to the scattering and will cause a decrease of lifetimes. This is consistent with the observed trend for face dependence of hot-electron scattering above 2 eV, with the most open face, Cu(110), having the fastest rates. Band structure calculations based on LDA are known to result in  $d$ -band energy positions that are slightly higher ( $\sim 0.2$  eV in the present case) than the experiment.<sup>52,53</sup> Thus, the agreement between the calculated and observed threshold energy for hot-electron scattering in Cu(110) may in part be due to cancellation of errors in the calculated  $d$ -band maximum of the bulk and its actual position at the surface. Another face-dependent difference in surface density of states is due to the existence of occupied crystal-induced surface states and resonances near the Fermi level of all three faces.<sup>54</sup> Thus, the surface electronic structure is specific to each surface and considerably different from the bulk, and therefore, it may contribute to the anisotropy of the observed rates.

The fact that the best agreement between theory and experiment is obtained for Cu(110), where no band gap exists in the  $k_{\parallel}=0$  direction ( $\Gamma$ - $K$ ), suggests the band gaps at Cu(111) and Cu(100) may be responsible for the deviations from the predictions of the Fermi-liquid theory. The nature of the intermediate states, whose lifetime is measured in the band gap of Cu(111) and Cu(100), is not known. The band-gap photoemission may be from damped band-gap states, phonon assisted transitions, and contribution of  $k_{\parallel} \neq 0$  photoemission due to final-state scattering and finite acceptance

angle of the analyzer.<sup>10</sup> Some DOS in the band gap may be due to nonremovable defects such as steps or surface impurities, since the photoemission signal increases when the surface is sputtered or exposed to oxygen. The lifetime of the band-gap states is determined by the penetration depth of the wave function into the bulk.<sup>33,55,56</sup> Thus, the lifetimes of the surface states in the band gap are slower than for the bulk. A strong surface contribution to the band-gap photoemission for Cu(100) and Cu(111) could explain the anisotropy of the rates and deviations from the calculated hot-electron scattering rates for the bulk.

## V. SUMMARY

Hot-electron lifetimes are measured for three low-index Cu surfaces with <10 fs resolution. The lifetimes do not follow the  $(E - E_F)^{-2}$  dependence predicted by the Fermi-liquid theory for free-electron metals and have a crystal face dependence. A numerical calculation of  $e-e$  scattering rates based on Cu band structure reproduces qualitatively the energy dependence of the hot-electron lifetimes with particularly good agreement for Cu(110). It is shown that the deviation from the  $(E - E_F)^{-2}$  dependence is mainly due to participation of the  $d$  bands in scattering of >2 eV hot electrons. However, magnitudes of experimental lifetimes are still  $\sim 6$  times slower than those calculated. The overestima-

tion of the rates is attributed to several assumptions in calculating the rates, including the Born approximation, and neglect of exchange interaction (assumption of spin-independent scattering),  $d$ -band screening, and umklapp processes. Errors introduced by these assumptions are of sufficient magnitude to explain the overestimation of the  $e-e$  scattering rates. The band-structure calculation shows much smaller differences in the scattering rates for the low index faces of Cu than the experiment. The crystal face dependence of lifetimes may reflect the anisotropy in the  $e-e$  and  $e-p$  scattering cross sections or face-dependent differences in the surface electronic structure. Further refinement of our knowledge of hot-electron dynamics at metal surfaces requires a better understanding of coherent and incoherent dynamics involved in the two-photon photoemission process, more realistic models for fitting the hot-electron population dynamics, including effects due to the hot-electron cascade, diffusion, and  $e-p$  scattering, and more sophisticated theoretical models for calculating the  $e-e$  scattering rates.

## ACKNOWLEDGMENTS

The authors would like to thank S. Matsunami and N. Moriya for technical support, and E. Murayama for valuable discussions regarding theoretical aspects of this work.

- 
- <sup>1</sup>R. R. Cavanagh, D. S. King, J. C. Stephenson, and T. F. Heinz, *J. Phys. Chem.* **97**, 786 (1993).
- <sup>2</sup>P. M. Lee, T. Garfinkel, P. K. Ko, and C. Hu, *IEEE Trans. Electron Devices* **41**, 852 (1994).
- <sup>3</sup>S. Y. Chu and M. Y. Liu, *IEEE J. Quantum Electron.* **28**, 2538 (1992).
- <sup>4</sup>R. G. Sharpe, St. J. Dixon-Warren, P. J. Durston, and R. E. Palmer, *Chem. Phys. Lett.* **234**, 354.
- <sup>5</sup>J. W. Gadzuk, *Phys. Rev. Lett.* **76**, 4234 (1996).
- <sup>6</sup>M. Kaveh and H. Wisner, *Adv. Phys.* **33**, 257 (1984).
- <sup>7</sup>B. A. McDougall, T. Balasubramanian, and E. Jensen, *Phys. Rev. B* **51**, 13 891 (1995); R. Paniago, R. Matzdorf, G. Meister, and A. Goldmann, *Surf. Sci.* **331-333**, 1233 (1995).
- <sup>8</sup>R. H. M. Groeneveld, R. Spirk, and A. Lagendijk, *Phys. Rev. B* **45**, 5079 (1991); C. Suárez, W. E. Bron, and T. Juhasz, *Phys. Rev. Lett.* **75**, 4536 (1995).
- <sup>9</sup>C. K. Sun *et al.*, *Phys. Rev. B* **50**, 15 337 (1994).
- <sup>10</sup>S. Ogawa and H. Petek, *Surf. Sci.* **357-358**, 585 (1996).
- <sup>11</sup>J. Bokor, *Science* **246**, 1130 (1989); R. Haight, *Surf. Sci. Rep.* **21**, 275 (1995).
- <sup>12</sup>W. S. Fann, R. Storz, H. W. K. Tom, and J. Bokor, *Phys. Rev. B* **46**, 13 592 (1992).
- <sup>13</sup>C. A. Schmuttenmaer, M. Aeschlimann, H. E. Elsayed-Ali, R. J. D. Miller, D. A. Mantell, J. Cao, and Y. Gao, *Phys. Rev. B* **50**, 8957 (1994).
- <sup>14</sup>M. Aeschlimann, M. Bauer, and S. Pawlik, *Chem. Phys.* **205**, 127 (1996).
- <sup>15</sup>T. Hertel, E. Knoesel, M. Wolf, and G. Ertl, *Phys. Rev. Lett.* **76**, 535 (1996).
- <sup>16</sup>R. L. Lingle, Jr., N.-H. Ge, R. E. Jordan, J. D. McNeil, and C. B. Harris, *Chem. Phys.* **205**, 191 (1996).
- <sup>17</sup>R. W. Schoenlein, J. G. Fujimoto, G. L. Eesley, and T. W. Capehart, *Phys. Rev. B* **43**, 4688 (1991).
- <sup>18</sup>J. J. Quinn, *Phys. Rev.* **126**, 1453 (1962).
- <sup>19</sup>J. B. Smith and H. Ehrenreich, *Phys. Rev. B* **25**, 923 (1982); W. P. Dumke, *Phys. Rev.* **124**, 1813 (1961).
- <sup>20</sup>S. Ogawa and H. Petek, *Surf. Sci.* **363**, 313 (1996).
- <sup>21</sup>B. Quiniou, V. Bulovic, and R. M. Osgood, Jr., *Phys. Rev. B* **47**, 15 890 (1993).
- <sup>22</sup>K. Giesen, F. Hage, F. J. Himpsel, H. J. Riess, and W. Steinmann, *Phys. Rev. B* **35**, 971 (1987).
- <sup>23</sup>D. Rieger, T. Wegehaupt, and W. Steinmann, *Phys. Rev. Lett.* **58**, 1135 (1987).
- <sup>24</sup>F. Weik, A. de Meijere, and E. Hasselbrink, *J. Chem. Phys.* **99**, 682 (1993).
- <sup>25</sup>H. P. Weber and H. G. Danielmeyer, *Phys. Rev. A* **2**, 2074 (1970).
- <sup>26</sup>S. Ogawa and H. Petek, in *Quantum Coherence and Decoherence*, edited by K. Fujikawa and Y. A. Ono (North-Holland, Amsterdam, 1996), pp. 203–206.
- <sup>27</sup>S. Ogawa, H. Nagano, H. Petek, and A. P. Heberle, *Phys. Rev. Lett.* (to be published).
- <sup>28</sup>J. M. Ziman, *Electrons and Phonons* (Clarendon, Oxford, 1960).
- <sup>29</sup>V. A. Gasparov and R. Huguenin, *Adv. Phys.* **42**, 393 (1993).
- <sup>30</sup>D. Pines and P. Nozieres, *The Theory of Quantum Liquids* (Benjamin, New York, 1966).
- <sup>31</sup>O. Gunnarsson and B. I. Lundqvist, *Phys. Rev. B* **13**, 4274 (1976).
- <sup>32</sup>G. A. Burdick, *Phys. Rev.* **129**, 138 (1963).
- <sup>33</sup>Th. Fauster and W. Steinmann, in *Electromagnetic Waves: Recent Developments in Research*, edited by P. Halevi (North-Holland, Amsterdam, 1995), Vol. 2, pp. 347–411.
- <sup>34</sup>N. W. Aschcroft and N. D. Mermin, *Solid State Physics* (Holt,

- Reinhart, and Winston, New York, 1966).
- <sup>35</sup>O. B. Wright and V. E. Gusev, *Physica B* **219-220**, 770 (1996).
- <sup>36</sup>M. Springford, *Adv. Phys.* **20**, 493 (1971).
- <sup>37</sup>D. A. Shirley, *Phys. Rev. B* **5**, 4709 (1972); T. Miller, W. E. McMahon, and T.-C. Chiang, *Phys. Rev. Lett.* **77**, 1167 (1996).
- <sup>38</sup>More recent measurements by J. Cao, C. Cameron Miller, R. J. D. Miller, H. E. Elasyed-Ali, D. A. Mantell, and Y. Gao, *Phys. Rev. B* (to be published) are in significantly better agreement with the results reported here.
- <sup>39</sup>C. R. Crowell and S. M. Sze, *Physics of Thin Films* (Academic, New York, 1967), Vol. 4.
- <sup>40</sup>K. El Sayed, L. Banyai, and H. Haug, *Phys. Rev. B* **50**, 1541 (1994); J. R. Kuklinski and S. Mukamel, *ibid.* **44**, 11 253 (1991).
- <sup>41</sup>H. Haug and S. W. Koch, *Quantum Theory of the Optical and Electronic Properties of Semiconductors* (World Scientific, Singapore, 1990).
- <sup>42</sup>R. W. Davies, *Phys. Rev.* **181**, 1118 (1969).
- <sup>43</sup>C. A. Kukkonen and H. Smith, *Phys. Rev. B* **8**, 4601 (1973).
- <sup>44</sup>D. R. Penn, *Phys. Rev. B* **22**, 2677 (1980); R. H. Ritchie and J. C. Ashley, *J. Phys. Chem. Solids* **26**, 1689 (1965).
- <sup>45</sup>E. Beaupaire, J.-C. Merle, A. Daunois, and J.-Y. Bigot, *Phys. Rev. Lett.* **76**, 4250 (1996).
- <sup>46</sup>H. Ehrenreich and H. R. Philipp, *Phys. Rev.* **128**, 1622 (1962).
- <sup>47</sup>J. J. Quinn, *Appl. Phys. Lett.* **2**, 167 (1963).
- <sup>48</sup>S. L. Adler, *Phys. Rev.* **130**, 1654 (1963).
- <sup>49</sup>H. Stubi, P.-A. Probst, R. Huguenin, and V. A. Gasparov, *J. Phys. F* **18**, 1211 (1988).
- <sup>50</sup>S. G. Das, *Phys. Rev. B* **7**, 2238 (1973).
- <sup>51</sup>D. G. Dempsey and L. Kleinman, *Phys. Rev. B* **16**, 5356 (1977); A. Euceda, D. M. Bylander, L. Kleinman, and K. Mednick, *ibid.* **27**, 659 (1983); A. Euceda, D. M. Bylander and L. Kleinman, *ibid.* **28**, 528 (1983).
- <sup>52</sup>O. Jepsen, D. Glotzel, and A. R. Mackintosh, *Phys. Rev. B* **23**, 2684 (1981).
- <sup>53</sup>J. A. Knapp, F. J. Himpsel, and D. E. Eastman, *Phys. Rev. B* **19**, 4952 (1979).
- <sup>54</sup>W. Jacob, V. Dose, U. Kolac, Th. Fauster, and A. Goldmann, *J. Phys.* **63**, 459 (1986).
- <sup>55</sup>P. de Andres, P. M. Echenique, and F. Flores, *Phys. Rev. B* **35**, 4529 (1987).
- <sup>56</sup>S. Scheppler, N. Fischer, Th. Fauster, and W. Steinmann, *Phys. Rev. B* **46**, 13 539 (1992).